

Magnetic Resonance Spectroscopy Quantification Aided by Deep Estimations of Imperfection Factors and Overall Macromolecular Signal

Dicheng Chen[#], Meijin, Lin[#], Huiting Liu, Jiayu Li, Yirong Zhou, Taishan Kang, Liangjie Lin, Zhigang Wu, Jiazheng Wang, Jing Li, Jianzhong Lin, Xi Chen, Di Guo and Xiaobo Qu*

Abstract—Magnetic Resonance Spectroscopy (MRS) is an important non-invasive technique for *in vivo* biomedical detection. However, it is still challenging to accurately quantify metabolites with proton MRS due to three problems: Serious overlaps of metabolite signals, signal distortions due to non-ideal acquisition conditions and interference with strong background signals including macromolecule signals. The most popular software, LCModel, adopts the non-linear least square to quantify metabolites and addresses these problems by introducing regularization terms, imperfection factors of non-ideal acquisition conditions, and designing several empirical priors such as basis-sets of both metabolites and macromolecules. However, solving such a large non-linear quantitative problem is complicated. Moreover, when the signal-to-noise ratio of an input MRS signal is low, the solution may have a large deviation. In this work, deep learning is introduced to reduce the complexity of solving this overall quantitative problem. Deep learning is designed to predict directly the imperfection factors and the overall signal from macromolecules. Then, the remaining part of the quantification problem becomes a much simpler effective fitting and is easily solved by Linear Least Squares (LLS), which greatly improves the generalization to unseen concentration of metabolites in the training data. Experimental results show that compared with LCModel, the proposed method has smaller quantification errors for 700 sets of simulated test data, and presents more stable quantification results for 20 sets of healthy *in vivo* data at a wide range of signal-to-noise ratio. QNet also outperforms other deep learning methods in terms of lower quantification error on most metabolites. Finally, QNet has been deployed on a cloud computing platform, CloudBrain-MRS, which is open accessed at <https://csrc.xmu.edu.cn/CloudBrain.html>.

Index Terms—Deep learning, imperfection factors, macromolecules, magnetic resonance spectroscopy, metabolite quantification, least squares.

I. INTRODUCTION

MAGNETIC Resonance Spectroscopy (MRS) is a technique for non-invasive detection of biochemical

This work was partially supported by the National Natural Science Foundation of China (62122064, 61971361, 61871341), the Natural Science Foundation of Fujian Province of China (2021J011184), the President Fund of Xiamen University (20720220063), and Nanqiang Outstanding Talent Program of Xiamen University.

D. Chen, H. Liu, Y. Zhou, Jiayu Li and X. Qu are with Department of Electronic Science, Fujian Provincial Key Laboratory of Plasma and Magnetic Resonance, Xiamen University, Xiamen 361005, China

M. Lin is with Department of Applied Marine Physics and Engineering, and Fujian Provincial Key Laboratory of Plasma and Magnetic Resonance, Xiamen University, Xiamen 361102, China.

metabolites in living tissues [1]. It has been clinically used to identify changes in metabolite levels in regions of interest (e.g., brain [2], spinal cord [3], liver [4] and other organs [5]) of *in vivo*. Thus, MRS has great scientific and clinical value for the diagnosis, and therapeutic follow-up of genetic, oncological and degenerative diseases. However, the quantification of metabolites in proton MRS (¹H-MRS) is rather complicated. This is because of serious overlaps of metabolite signals, signal distortions due to non-ideal acquisition conditions and interference with background signal that are mostly contributed by MacroMolecules (MMs). How to handle the above problems will be briefly discussed below.

Highly overlapped signals of metabolites are due to the narrow spectral dispersion caused by the limited magnetic field strength in a clinical magnetic resonance scanner. To improve the quantification, a direct way is introducing empirical prior of each metabolite signal. As a most recognized quantification method, LCModel [6] designed a basis-set of metabolic profiles to calculate the contribution of individual metabolites to an observed spectrum of multiple metabolites. The basis-set was acquired from a high-field scanner through time-consuming *in vitro* experiments and may introduce experimental errors (e.g. effects of temperature, pH, etc.) [1, 7]. These errors need correction through complicated processing to adapt the basis-set to *in vivo* human spectrum [7]. In another way, without any real scanning, the quantification errors [8, 9] could be reduced by using the simulated basis-set [10]. Through the Quantum Mechanical and Exponential Model (QMEM), each metabolite signal can be generated according to the actual pulse sequence parameters, the *in vivo* environments (e.g., MM or lipid signals) and Imperfection Factors (IFs) of non-ideal acquisition conditions (e.g., deviations of phase, frequency, linewidth, etc.). Current QMEM MRS tools include FID-A [11], GAMMA [10], NMR-SCOPE [12], etc.

IFs of non-ideal acquisition conditions are commonly

L. Lin, Z. Wu, and J. Wang are with Philips, Beijing 100016, China.
Jing Li is with Xingaoyi Medical Equipment Company, Yuyao 315400, China.

T. Kang and J. Lin are with Department of Radiology, Zhongshan Hospital affiliated to Xiamen University, Xiamen 361004, China.

X. Chen is with the McLean Hospital, Harvard Medical School, Belmont, MA 02478, USA.

D. Guo is with School of Computer and Information Engineering, Xiamen University of Technology, Xiamen 361024, China.

[#]D. Chen and M. Lin are equally contributed to this work.

*Corresponding author with email: quxiaobo@xmu.edu.cn

> REPLACE THIS LINE WITH YOUR MANUSCRIPT ID NUMBER (DOUBLE-CLICK HERE TO EDIT) <

mathematically modelled using nonlinear factors [13]. For MRS, three main nonlinear factors are commonly considered. 1) Phase shift due to the dominating zero-order phase misadjustment from the phase difference between the excitation and the detection [14]; 2) Frequency shift due to scanner frequency shift, magnetic field inhomogeneity, tissue heterogeneity and variation, subject movement or physiological motion, etc. [15]; 3) Linewidth deviation due to magnetic field inhomogeneity, etc. [16]. Linewidth is represented as full-width at half-maximum. Thus, quantitative estimation is commonly addressed by solving the non-linear least square problems [17], which are relatively complicated and many introduce large errors when the Signal-to-Noise Ratio (SNR) of the input signal is low [15].

MM signal is constituted of all rapidly relaxing signals that have not decayed to zero at the chosen Echo Time (TE). In this work, we also simulated the MM signal by QMEM with Gaussian functions [13, 18].

The quantification tools, such as LCModel [6], QUEST [19], AQSES [20] and TARQUIN [21] etc., developed a measurement of quantitative estimation by designing more empirical priors, constraint conditions and regularizations. However, the process of solving such a large quantitative object is still complicated. With the simulated data test, LCModel was shown that the fitting bias, i.e., the deviation from true values, increases as SNR decreases [22].

Recently, deep learning has made significant progress in MRS processing [9, 13, 18, 23-31]. Its database learning with labels has directly and successfully quantified metabolite concentrations from input spectrum, especially from low SNR spectrum, in an end-to-end manner [18, 27, 29, 31]. However, the end-to-end strategy has limited generalization, and thus the network should be retrained if any metabolite concentration for the test is out of the range from the trained data [18, 23].

In this work, we designed an MRS Quantification neural Network (QNet) with two modules to extract the IFs and overall MM signal. Rather than using end-to-end deep learning, QNet employs Linear Least Squares (LLS) aided by the deep neural network of the two modules to quantify metabolite concentrations. We applied the QMEM to synthesize the basis-set and incorporate *in vivo* parameter information to form many spectra to train QNet. Both simulation and *in vivo* experiments were conducted to compare QNet with LCModel. The former experiments show that QNet can achieve more accurate quantification and be more robust to noise. The latter experiments demonstrate that the quantification results of QNet and LCModel are consistent when SNR is high, whereas QNet can be more stable when SNR decreases.

The rest of this paper is organized as follows: Sections II, III and IV present the proposed method, network implementation, and prepared data, respectively. Section V provides the main results. Section VI discusses the limitations and Section VII concludes this work.

II. METHOD

This section describes the proposed method that estimates the

non-ideal acquisition factors and overall MM signal with deep learning, and then linearly estimates the metabolic concentration.

A schematic diagram of determining the contributions of individual metabolites to the total MRS signal is shown in Fig. 1. The real matrix \mathbf{M} is the basis-set including individual metabolites. The detected spectrum $\mathbf{y} = \mathbf{M}\mathbf{c} + \boldsymbol{\varepsilon}$ is modeled as the sum of additive Gaussian noise $\boldsymbol{\varepsilon}$ and linear combination with the concentration \mathbf{c} of individual metabolites. Concentration \mathbf{c} could be estimated through solving the LLS problem:

$$\hat{\mathbf{c}} = \arg \min_{\mathbf{c}} \|\mathbf{M}\mathbf{c} - \mathbf{y}\|_2^2, \quad (1)$$

where $\|\cdot\|_2$ is the l_2 norm of a vector, and $\hat{\mathbf{c}}$ is the estimated concentration. Equation (1) is effective since it has analytical solution $\hat{\mathbf{c}} = (\mathbf{M}^H \mathbf{M})^\dagger \mathbf{M}^H \mathbf{y}$ where H is the Hermitian transpose and † is the pseudo inverse. Besides, the solution $\hat{\mathbf{c}}$ is a minimum-variance unbiased estimation because $\boldsymbol{\varepsilon}$ is homoscedastic and uncorrelated to $\mathbf{M}\mathbf{c}$.

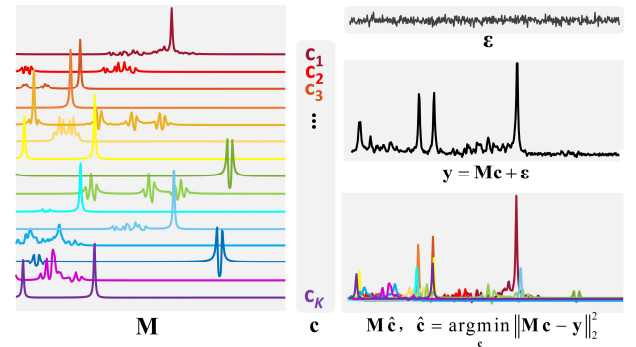


Fig. 1. Schematic diagram of basic spectrum fitting for quantification. Notes: \mathbf{M} is the metabolite basis-set, $\boldsymbol{\varepsilon}$ is the additive Gaussian noise, \mathbf{y} is the detected spectrum, $\hat{\mathbf{c}}$ is the solution obtained by LLS (an unbiased estimation of concentration), and $\mathbf{M}\hat{\mathbf{c}}$ is the fitted spectrum.

In practice, IFs including phase shift $\Delta\phi$, frequency shift Δf and linewidth deviation Δd should be considered in the quantification. Accordingly, (1) is modified as:

$$\min_{\mathbf{c}, \Delta\phi, \Delta f, \Delta d} \|\mathbf{M}'\mathbf{c} - \mathbf{y}\|_2^2, \quad \mathbf{M}' = h(\mathbf{M}, \Delta\phi, \Delta f, \Delta d), \quad (2)$$

where the function $h(\mathbf{M}, \Delta\phi, \Delta f, \Delta d)$ is the modulation of \mathbf{M} by IFs $\{\Delta\phi, \Delta f, \Delta d\}$. In addition to the more difficulty to find the solution, the IFs $\{\Delta\hat{\phi}, \Delta\hat{f}, \Delta\hat{d}\}$ extracted from the input \mathbf{y} by this nonlinear least square estimation of (2) have large errors when the SNR of the input signal \mathbf{y} is low [15].

In the proposed QNet, we designed a neural network module to extract the IFs (upper part of Fig. 2b), and the difficulty of solving (2) is reduced by deep learning:

$$\mathcal{N}_{\text{extraction}}(\hat{\mathbf{y}} | \Theta_{\text{extraction}}) = \{\Delta\hat{\phi}, \Delta\hat{f}, \Delta\hat{d}\} \quad (3)$$

$$\min_{\mathbf{c}} \|\mathbf{M}(\mathbf{M}, \Delta\hat{\phi}, \Delta\hat{f}, \Delta\hat{d})\mathbf{c} - \mathbf{y}\|_2^2$$

where $\mathcal{N}_{\text{extraction}}(\mathbf{y} | \Theta_{\text{extraction}})$ is the deep learning model for

> REPLACE THIS LINE WITH YOUR MANUSCRIPT ID NUMBER (DOUBLE-CLICK HERE TO EDIT) <

extracting the IFs from the input \mathbf{y} with the trainable network parameters $\Theta_{\text{extraction}}$, and $\{\Delta\hat{\varphi}, \Delta\hat{\mathbf{f}}, \Delta\hat{d}\}$ is the predicted IFs. Once these IFs have been obtained, estimating \mathbf{c} becomes an easy LLS problem and a closed-form solution can be achieved.

The background signal from MMs should also be considered. So, the parametric model for MMs should be added to solve (2), further exacerbating the difficulty of solving the quantification:

$$\min_{\mathbf{c}, \Delta\varphi, \Delta\mathbf{f}, \Delta d, \lambda, \Omega} \|h(\mathbf{M}, \Delta\varphi, \Delta\mathbf{f}, \Delta d)\mathbf{c} - \mathbf{y} + \lambda\mathbf{b}(\Omega)\|_2^2, \quad (4)$$

where \mathbf{b} is the background signal from MMs with a structure parameter Ω and an intensity λ . Similar to the recent research [29], another deep learning module (lower part of Fig. 2b) is designed in QNet to predict the overall MM signal $\hat{\mathbf{b}}$ which is then subtracted from \mathbf{y} . This can reduce the burden of quantitative estimation in (4):

$$\begin{aligned} \mathcal{N}_{\text{prediction}}(\mathbf{y} | \Theta_{\text{prediction}}) &= \hat{\mathbf{b}} \\ \min_{\mathbf{c}, \Delta\varphi, \Delta\mathbf{f}, \Delta d} \|h(\mathbf{M}, \Delta\varphi, \Delta\mathbf{f}, \Delta d)\mathbf{c} - \mathbf{y} + \hat{\mathbf{b}}\|_2^2, \end{aligned} \quad (5)$$

where $\mathcal{N}_{\text{prediction}}(\mathbf{y} | \Theta_{\text{prediction}})$ is a deep learning module for predicting \mathbf{b} from the input \mathbf{y} with parameters $\Theta_{\text{prediction}}$.

In summary, three steps are required in QNet: 1) Estimating IFs by solving (3); 2) Obtaining the overall MM signal by solving (5). 3) Estimating metabolite concentrations via the LLS problem between the basis-set with IFs and the remaining signal after deduction of the overall MM signal. These steps are expressed as follows:

$$\begin{aligned} \mathcal{N}_{\text{extraction}}(\mathbf{y} | \Theta_{\text{extraction}}) &= \{\Delta\hat{\varphi}, \Delta\hat{\mathbf{f}}, \Delta\hat{d}\} \\ \mathcal{N}_{\text{prediction}}(\mathbf{y} | \Theta_{\text{prediction}}) &= \hat{\mathbf{b}} \\ \min_{\mathbf{c}} \|h(\mathbf{M}, \Delta\hat{\varphi}, \Delta\hat{\mathbf{f}}, \Delta\hat{d})\mathbf{c} - \mathbf{y} + \hat{\mathbf{b}}\|_2^2 \end{aligned} \quad (6)$$

III. IMPLEMENTATION OF QNET

Fig. 2 shows the procedure of QNet, which includes: 1) Synthesizing training data; 2) Training two deep learning modules that determine IFs and the overall MM signal from

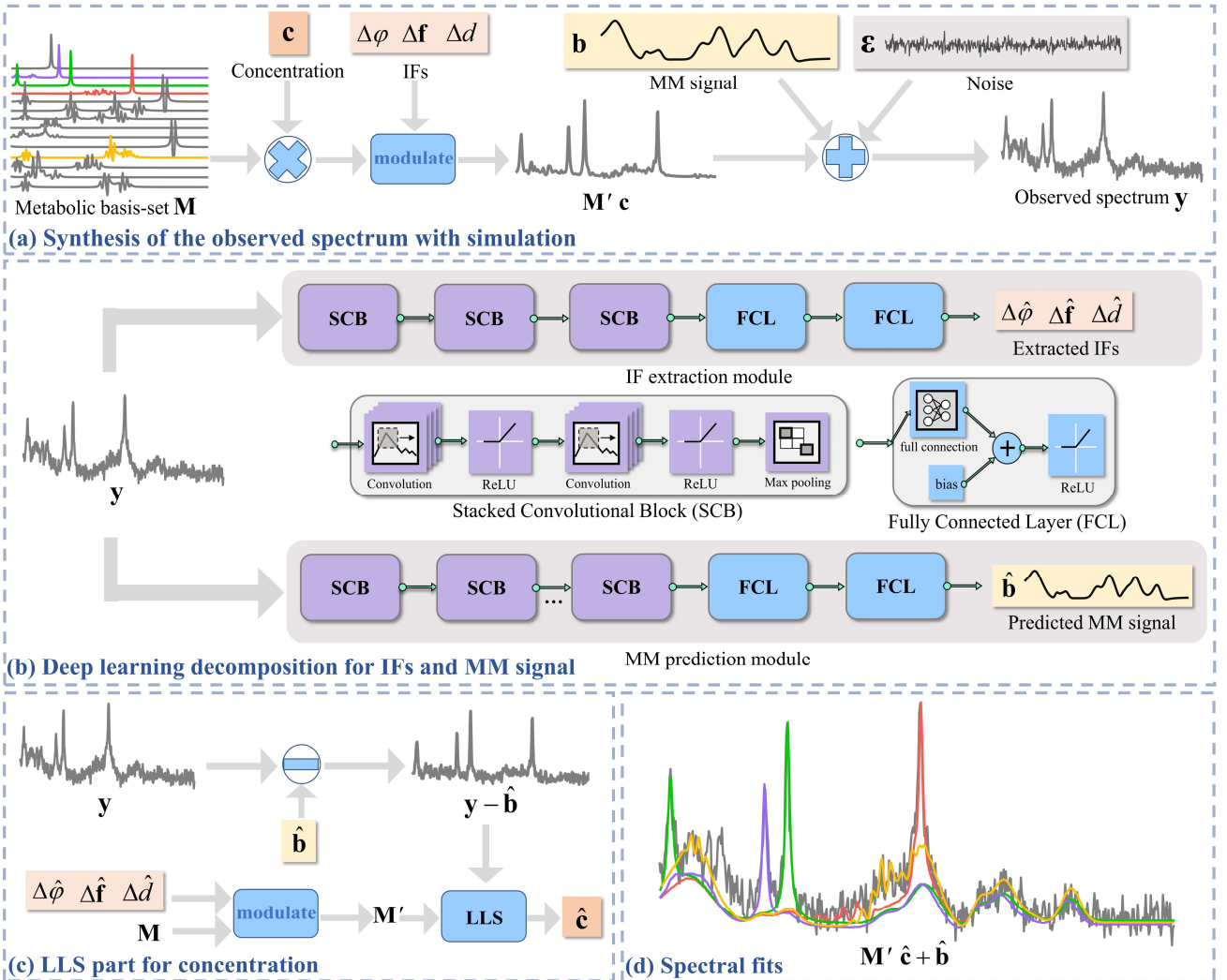


Fig. 2. The procedure of QNet: (a) Procedure of spectrum synthesis, (b) deep learning part with two modules to extract IFs and the overall MM signal, respectively, (c) LLS part using the estimate results from (b) to predict metabolite concentration, and (d) fitted spectrum by combining the results of deep learning from (b) and LLS from (c).

> REPLACE THIS LINE WITH YOUR MANUSCRIPT ID NUMBER (DOUBLE-CLICK HERE TO EDIT) <

input, respectively; 3) Estimating metabolite concentrations with LLS.

A. Synthetic Data Generation with QMEM

We resorted to synthetic data to train the network since it is impossible to obtain the true values of the IFs and the concentrations from detected *in vivo* MRS data. Synthetic data will be generated following the physical law and this strategy has been observed powerful in deep learning processing of spectroscopy [8, 9, 30]. A complex sampling point of the MRS signal \mathbf{y} is generated according to:

$$\hat{\mathbf{y}}(n\Delta t) = \sum_{k=1}^K c_k h_k(m_k(n\Delta t) | \boldsymbol{\theta}_k) + b(n\Delta t) + \varepsilon(n\Delta t), \quad (7)$$

$$n = 0, 1, 2, \dots, N-1$$

where $N, \Delta t, K$ denotes the length of the signal, the sampling interval and the number of metabolites, respectively; c_k is the k^{th} concentration; $\varepsilon(n\Delta t)$ is the complex white Gaussian noise [32]; $b(n\Delta t)$ represents the complex total signal from MMs; and $h_k(m_k(n\Delta t) | \boldsymbol{\theta}_k)$ denotes the k^{th} metabolite component signal modulated with the IFs $\boldsymbol{\theta}_k = \{\Delta\varphi, \Delta f_k, \Delta d\}$, and is expressed as:

$$h_k(m_k(n\Delta t) | \boldsymbol{\theta}_k) = e^{i\Delta\varphi} m_k(n\Delta t) e^{(i2\pi\Delta f_k - \Delta d)n\Delta t}, \quad (8)$$

$$n = 0, 1, 2, \dots, N-1$$

where i denotes the imaginary unit and satisfies $i^2 = -1$, $\boldsymbol{\theta}_k$ is the set of the IFs (including zero-order phase drift $\Delta\varphi$, frequency drift Δf_k and linewidth deviation Δd) of the k^{th} metabolite, and $m_k(n\Delta t)$ denotes the n^{th} point of ideal MRS time-domain signal of the k^{th} metabolite. The corresponding frequency-domain of $m_k(n\Delta t)$ is the point of the n^{th} row and k^{th} column of the basis set matrix \mathbf{M} , which is generated by FID-A based on QMEM [11].

B. Extraction of Imperfection Factors

This module consists of 3 Stacked Convolutional Blocks (SCBs) and 2 Fully Connected Layers (FCLs). The 3 SCBs all contain 2 convolutional layers and use respectively 16, 32 and 64 filters with the same kernel size of 3×1 . After the convolution operation, the non-linear activation function Rectified Linear Unit (ReLU) is followed, and then the maximum pooling is performed. The module finally outputs a 1D vector containing a set of IFs for all the target metabolites. The structure of this module is shown in the upper part of Fig. 2b, and the detailed structures of an SCB and an FCL are shown in the middle of Fig. 2b. The overall process of the IF extraction module can be expressed as:

$$\mathcal{N}_{\text{extraction}}(\mathbf{y} | \Theta_{\text{extraction}}) = \{\Delta\hat{\varphi}, \Delta\hat{\mathbf{f}}, \Delta\hat{d}\}, \quad (9)$$

where $\Theta_{\text{extraction}}$ represents the network parameters including 3 SCBs and 2 FCLs, and $\mathcal{N}_{\text{extraction}}(\mathbf{y} | \Theta_{\text{extraction}})$ represents the nonlinear extraction mapping from the detected spectrum \mathbf{y} to the IFs $\{\Delta\hat{\varphi}, \Delta\hat{\mathbf{f}}, \Delta\hat{d}\}$.

C. Estimation of Overall Macromolecule Signal

This module consists of 6 SCBs and 2 FCLs. The 6 SCBs all consist of 2 convolutional layers, and use 16, 32, 64, 128 and 256 filters, respectively, with the same kernel size of 3×1 . After the convolution operation, the ReLU activation function is followed, and then the maximum pooling is performed. The output of this module is a 1D vector of a size 512×1 as predicted MM signal. The structure of this module is shown in the lower part of Fig. 2b. The overall process of the MM prediction module can be expressed as:

$$\mathcal{N}_{\text{prediction}}(\mathbf{y} | \Theta_{\text{prediction}}) = \hat{\mathbf{b}}, \quad (10)$$

where $\Theta_{\text{prediction}}$ represents the network parameters of this module, and $\mathcal{N}_{\text{prediction}}(\mathbf{y} | \Theta_{\text{prediction}})$ represents the non-linear prediction mapping from the detected spectrum \mathbf{y} to the background MM signal $\hat{\mathbf{b}}$.

D. Estimation of Metabolite Concentrations

The LLS part (Fig. 2c) is designed to predict the metabolite concentrations, which are linear parameters in (1). Before the operation of LLS, the basis-set \mathbf{M} is updated to \mathbf{M}' via (8) with $\{\Delta\hat{\varphi}, \Delta\hat{\mathbf{f}}, \Delta\hat{d}\}$ that are determined by the IF extraction module, and the predicted MM signal $\hat{\mathbf{b}}$, which is subtracted from the detected signal \mathbf{y} . Therefore, the predicted concentration $\hat{\mathbf{c}}$ can be obtained by LLS:

$$\hat{\mathbf{c}} = (\mathbf{M}'^H \mathbf{M}')^{-1} \mathbf{M}'^H (\mathbf{y} - \hat{\mathbf{b}}). \quad (11)$$

As a result, the spectral fitting matrix $\hat{\mathbf{M}}$ containing all the individual metabolites is as:

$$\hat{\mathbf{M}} = \mathbf{M}' \odot \mathbf{C}, \quad (12)$$

where \odot represents the Hadamard product, $\mathbf{C} = \begin{bmatrix} \hat{\mathbf{c}}^T \\ \hat{\mathbf{c}}^T \\ \dots \end{bmatrix}_{N \times K}$ and H

is the transpose operation. The LLS module is expressed as:

$$\{\hat{\mathbf{c}}, \hat{\mathbf{M}}\} = \mathcal{N}_R(\{\Delta\hat{\varphi}, \Delta\hat{\mathbf{f}}, \Delta\hat{d}\}, \mathbf{M}, \hat{\mathbf{y}}, \hat{\mathbf{b}}). \quad (13)$$

Finally, the loss function is defined as:

$$Loss(\Theta) = \frac{1}{K} \|\hat{\mathbf{M}} - \mathbf{M}^{label}\|_F^2 + \alpha \|\hat{\mathbf{b}} - \mathbf{b}^{label}\|_F^2, \quad (14)$$

where $\Theta = \{\Theta_{\text{extraction}}, \Theta_{\text{prediction}}\}$ represents the set of overall network parameters, $\|\cdot\|_F$ is the Frobenius norm for a matrix, \mathbf{M}^{label} and \mathbf{b}^{label} are the training labels, and α is a weight to balance the two loss constraints.

IV. DATA PREPARATION

A. Parameter Ranges for Synthetic Data

Synthetic data were generated according to the prior ranges of metabolite signals, MM signals and IFs [18, 33, 34]. Details are listed below.

The number of metabolites, K in (7) is set to include the common brain metabolites. Their ranges of concentrations (mM) are set according to the literature [18, 33, 34] and listed here: N-acetylaspartate (NAA) (7.5-17), glutamate (Glu) (6.0-12.5), creatine (Cr) (4.5-10.5), Myo-Inositol (mI) (4.0-9.0),

> REPLACE THIS LINE WITH YOUR MANUSCRIPT ID NUMBER (DOUBLE-CLICK HERE TO EDIT) <

glutamine (Gln) (3.0-6.0), taurine (Tau) (2.0-6.0), phosphocreatine (PCr) (3.0-5.5), glutathione (GSH) (1.5-3.0), aspartate (Asp) (1.0-2.0), γ -aminobutyric acid (GABA) (1.0-2.0), glucose (Glc) (1.0-2.0), N-acetylaspartylglutamate (NAAG) (0.5-2.5), glycerophosphocholine (GPC) (0.5-2.0), phosphocholine (PCh) (0.5-2.0), alanine (Ala) (0.1-1.5), Lactate (Lac) (0.2-1.0), and scyllo-inositol (Scyllo) (0.3-0.6).

The overall MM signal is a synthesis of 17 MM signals, and each of them is modelled as a Gaussian function that has three parameters (chemical shift (ppm), amplitude (normalized to the largest last one), linewidth (Hz)). These parameters are (0.90, 0.72, 21), (1.20, 0.28, 19), (1.36, 0.38, 16), (1.63, 0.05, 8), (1.68, 0.05, 13), (1.81, 0.05, 13), (2.02, 0.78, 29), (2.08, 0.78, 21), (2.25, 0.78, 18), (2.97, 0.78, 5), (2.97, 0.3, 14), (3.11, 0.11, 18), (3.22, 0.11, 10), (3.27, 0.11, 10), (3.67, 0.71, 34), (3.80, 0.71, 12) and (3.96, 1, 37). To improve data generalization, their amplitudes and linewidths are randomly varied within $\pm 10\%$ and $\pm 20\%$, respectively. The ratio of the intensity of overall MM to overall metabolite signal is 0.15:1 and randomly varied within $\pm 25\%$. All the above parameters are referred to the literature [18, 35-37].

The ranges of the three IFs $\theta_k = \{\Delta\phi, \Delta f_k, \Delta d\}$ are [-5.00, 5.00] degree, [-0.08, 0.08] ppm, and [0.04, 0.12] ppm, respectively, all refer to the previous study [18].

Noise level is expressed by $\text{SNR} = \text{Amp}_{\text{NAA}} / \sigma_{\text{noise}}$, where Amp_{NAA} is the amplitude of the methyl peak of NAA at ~ 2.0 ppm, and σ_{noise} is the Standard Deviation (SD) of the spectral noise of 8.0-10.0 ppm. The SNR range is set as (0, 80] to cover that of 8 averages to 128 averages for *in vivo* data. A lower SNR means that the metabolite spectra (also called components) are contaminated more seriously by noise (first row of Fig. 3).

We simulated 60000 sets of MRS data for training and 700 for the test. Each set is amplitude normalized and cropped into 512 points in the range of 0.2 to 4.0 ppm.

B. In Vivo Data

All *in vivo* data were measured from the Philips 3T scanner with a 32-channel head coil. The fast spin-echo sequence was adopted to acquire T_1 -weighted brain images for voxel selection, and a point-resolved spectroscopy sequence [38] was used to acquire MRS data with an excitation module for water suppression [39]. Experimental parameters are: TR/TE= 2000 ms/ 35 ms, voxel size = 20 mm \times 20 mm \times 20 mm, number of data points= 2048, spectral bandwidth= 2000 Hz, Number of Signal Averages (NSA) = 128.

A total of 20 spectra were collected from 20 healthy subjects, respectively, in the following brain regions: 15 spectra from anterior or posterior frontal lobes, 1 from the parietal lobe, 1 from the occipital lobe and 3 from anterior or posterior cingulate gyrus. The human data acquisition was approved by the ethics committee of Xiamen University under Application No. XDYX202206K11.

V. RESULTS

To evaluate the performance, the proposed QNet is compared with other quantification methods, including the LCMoel and two state-of-the-art deep learning methods.

The quantification result of a target metabolite is represented by a relative concentration that is the ratio of the concentration of this metabolite to the concentration of the tCr (Cr + PCr).

A. Comparison with LCMoel on Simulated Data

Fig. 3 shows fitted spectra under representative high (first 2 columns) and low (last 2 columns) SNRs. When the SNR is high (SNR= 71.8), both QNet and LCMoel can achieve accurate fits visually since the residual of both methods are small. Besides, QNet obtains a lower residual, which indicates a better fit, than LCMoel. When the SNR is low (SNR= 20.0), both methods lead to strong residual and it is hard to judge which method is better.

To quantitatively compare the two methods, 100 sets of simulation data for each of the 7 SNR levels, that is 700 sets in total, were generated for the tests in Fig. 4. The estimated concentration of a component is directly compared with its ground truth value. Metabolites are listed in the ascending order (from left to right) of their true concentrations in the simulated data. The Mean Absolute Percentage Error (MAPE) is calculated as a criterion to evaluate quantification error:

$$\text{MAPE} = \frac{1}{I} \sum_{i=1}^I \frac{|c_i - \hat{c}_i|}{c_i}, \quad (15)$$

where I is the number of the data set with the same SNR level ($I = 100$ in this case), c_i is the ground truth value of the i -th set of data and \hat{c}_i is the estimation of c_i . A lower MAPE means more accurate quantification.

Fig. 4 shows that, for most metabolites, except for the too-low concentration metabolites (Ala, Asp, Lac, GABA), the MAPEs are smaller with QNet than with LCMoel. In particular, for NAAG, GPC, PCh and Gln, while LCMoel has large MAPEs close to 100%, QNet has significant improvement. Thus, QNet is a good quantification tool, and can even provide more accurate quantifications for many metabolites than LCMoel.

B. Comparison with LCMoel with In Vivo Data

Experiments on *in vivo* brain regions were also conducted to compare QNet to LCMoel qualitatively in Fig. 5 and quantitatively in Figs. 6-7 and Table I.

Fig. 5 shows the spectrum from an anterior frontal lobe with NSA=128 (high SNR). Both LCMoel and QNet have visually similar fitting results with the overall fits, their residuals and the estimations of the components (tNAA, tCr, tCho, Glx, ml and GSH). Both methods have fits of high quality with small residuals.

The consistency of estimated metabolite concentration between LCMoel and QNet is further assessed quantitatively with the Bland-Altman analysis using 20 *in vivo* spectra with NSA=128 (Fig. 6). First, one-sample T-test is performed with Standard Normal Distribution (SND) and the result of all p values > 0.05 is obtained, which means that the distribution of the 20 samples' differences is similar to SND and the systematic bias between the two methods is small. Second, because of $p > 0.05$ (satisfying normality), ± 1.96 SD can be used as the limits of agreement (dash line) to demonstrate a 95% confidence interval of the distributed data. Result shows that

> REPLACE THIS LINE WITH YOUR MANUSCRIPT ID NUMBER (DOUBLE-CLICK HERE TO EDIT) <

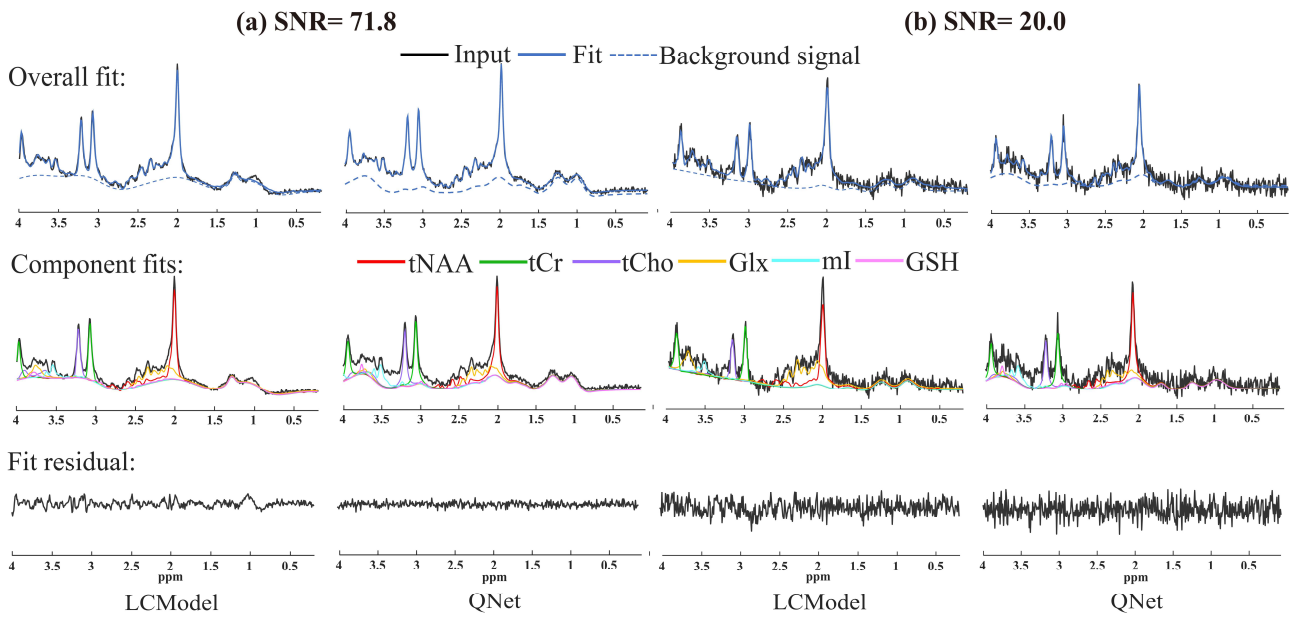
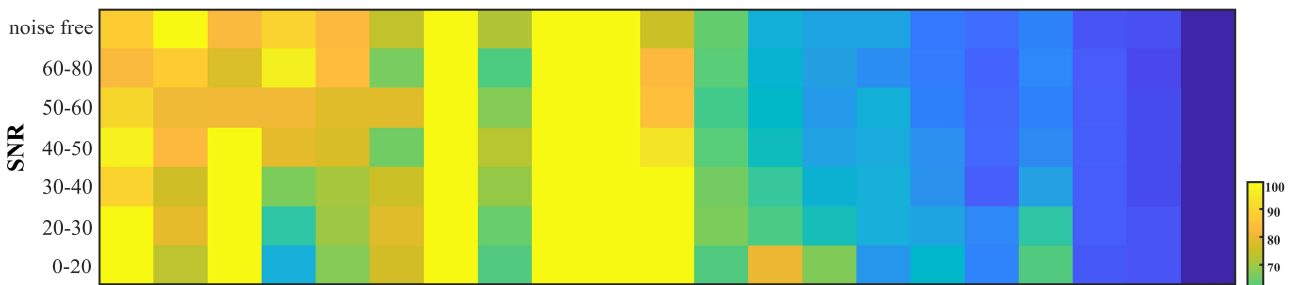


Fig.3. Spectral fits by LCMoDel and QNet on representative simulation at SNR of (a) 71.8 and (b) 20.0, respectively. The first row are the original input spectra (black solid line), the overall fit (blue solid line), and the estimated MM signal (blue dash line). The second row are the estimated individual spectra of the 6 main metabolites (tNAA, tCr, tCho, Glx, mI and GSH). The third row are the fitting residuals.

(a) MAPEs from LCMoDel



(b) MAPEs from QNet

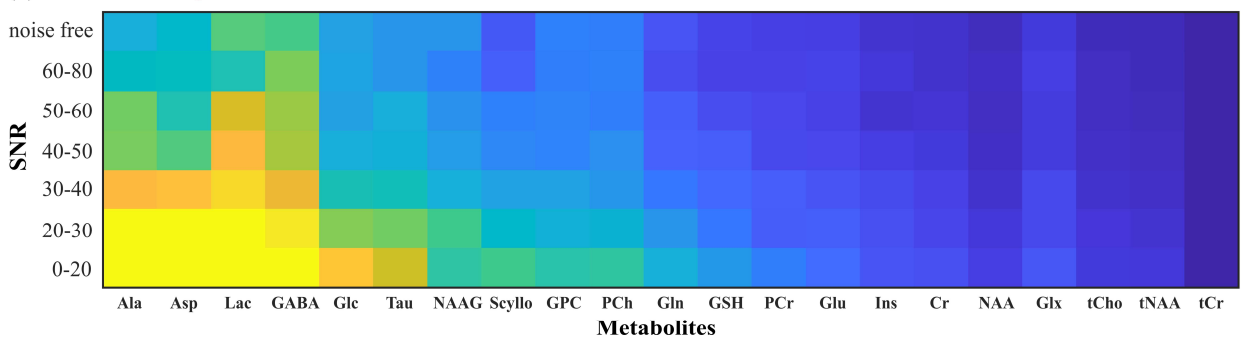


Fig. 4. The MAPEs of the estimated metabolite concentrations by (a) LCMoDel and (b) QNet at different SNRs. The blue color indicates lower error than the yellow one. From left to right, metabolites are listed in the ascending order of their true concentrations in simulated data.

95% or 90% of the data points are within the limits of agreement, which means good consistency between QNet and LCMoDel.

Fig. 7 compares the metabolite concentrations with boxplots estimated by QNet and LCMoDel from the 20 *in vivo* brain spectra. For tNAA, mI and Glx, both methods can acquire the estimated concentrations all within the normal ranges from [18, 33, 34]. For tCho, a few estimated concentrations reside outside of the upper limit with both methods. As for GSH, both methods get the worst results. Most of the results are outside of the

upper limit for LCMoDel, while QNet has better quantification with most of the values still within the limits.

Fig. 8 compares the metabolite quantification with different NSAs to imply the performance at different levels of noise for one *in vivo* data. Higher NSA means higher SNR since more averages are used at the cost of longer data acquisition time [23]. The SD is employed to evaluate the robustness of the two

> REPLACE THIS LINE WITH YOUR MANUSCRIPT ID NUMBER (DOUBLE-CLICK HERE TO EDIT) <

methods to different NSAs. Compared with LCModel, the concentrations estimated by QNet are generally more stable with smaller SDs. For Glx, the difference between the SDs of

the QNet (2.33) and LCModel (22.63) is very big, and the difference for GSH is big as well. Furthermore, the SDs of all the 20 *in vivo* MRS data with different NSA are listed in Table I, which means that QNet achieves smaller SDs for most of the MRS data than LCModel. Specifically, out of the 20 MRS data, QNet has 16, 17, 20, 19 and 17 smaller SDs for tNAA, mI, Glx, tCho and GSH, respectively. Therefore, QNet is more robust to different NSAs than LCModel.

D. Comparison with Other Deep Learning Methods

Table II compares QNet with two deep learning methods with simulation data. To make the comparison as fair as possible, the definitions of SNR and forecasting performance evaluation criteria from the reference are adopted. In [27], SNR is defined as $\text{SNR}_{\text{FID}} = [\text{iffit}(\mathbf{y})]_{\text{first}} / \sigma'_{\text{noise}}$, where $[\text{iffit}(\mathbf{y})]_{\text{first}}$ is the first point of time domain signal of spectrum \mathbf{y} , and σ'_{noise} is the SD of the noise in the time domain; and the Symmetric MAPE (SMAPE) [27] is used to measure the accuracy of the model for each metabolite and $\text{SMAPE} = \frac{1}{I} \sum_{i=1}^I \frac{|c_i - \hat{c}_i|}{c_i + \hat{c}_i}$. In [18], SNR is defined as

$\text{SNR}_x = \max(\mathbf{y}[x_k^1, x_k^2]) / \sigma'_{\text{noise}}$, where x is the target metabolite set $\{\text{tNAA}, \text{tCr}, \text{tCho}, \text{mI}, \text{Glx}\}$ and $[x_k^1, x_k^2]$ is the chemical shift range of k^{th} metabolite target peaks, and $\mathbf{y}[x_k^1, x_k^2]$ is the observed spectrum truncated within the chemical shift range.

Compared with the method from [27], QNet has a smaller SMAPE for all 9 metabolites listed in Table II. While compared

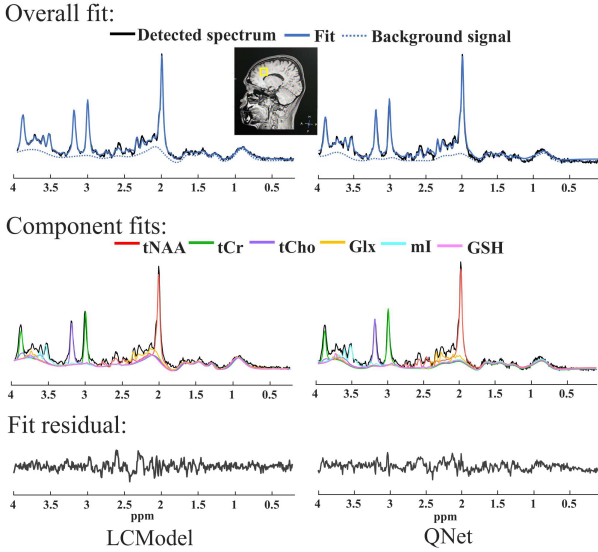


Fig. 5. Comparison between LCModel and QNet with one *in vivo* data from an anterior frontal lobe (in the yellow box). The first row are the original observed spectra (black solid line), the overall fit (blue solid line), and the estimated background signal (blue dash line). The second row are the contributions of the six highest components. The third row are the residuals.

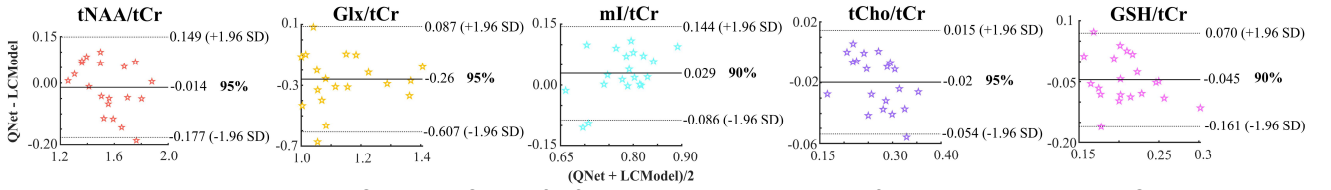


Fig. 6. Bland-Altman plots between the QNet and LCModel fits for the estimated concentrations from the 20 *in vivo* brain MRS data represented as 20 stars, respectively. The difference of the two measurements is plotted on the y axis, and the corresponding average on the x axis. The mean of the differences (solid line) is showed, and the limits of agreement (dashed lines) are calculated as mean \pm 1.96 SD. The percentage means the percent of the data points resides within the limits.

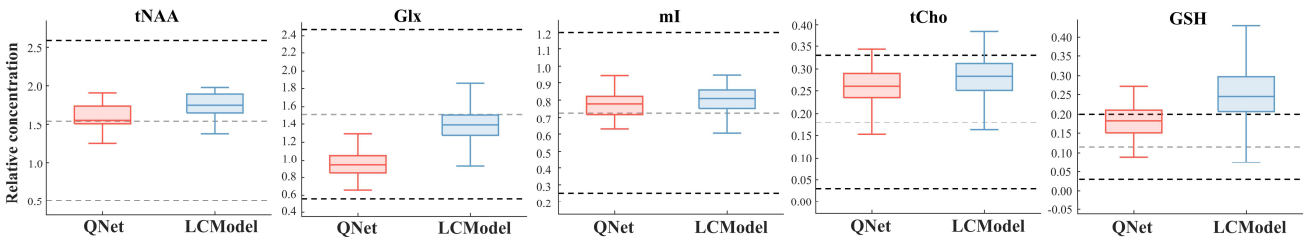


Fig. 7. Comparison of the relative concentrations estimated by QNet (red, left) and LCModel (blue, right) with box plots from the 20 *in vivo* brain spectra. Each box-plot contains 100×20 sets of data, specifically, 100 spectra with NSA of 124 are extracted randomly from each of the 20 fully sampled *in vivo* spectra with NSA of 128. The metabolite concentration range of normal human brain from the literature is marked with the dark dash lines and the mean value is marked with the light dash line.

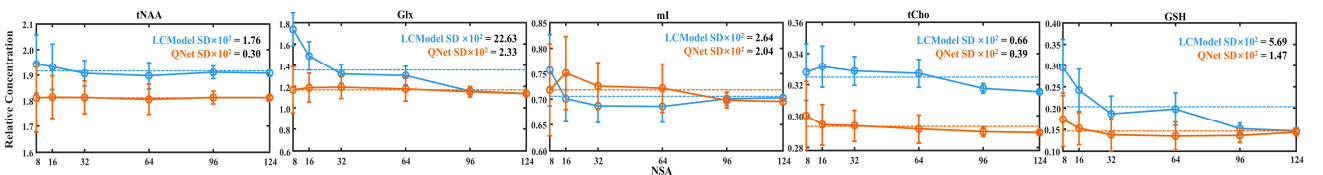


Fig. 8. Comparison of the relative concentrations estimated with different NSA by QNet (red) and LCModel (blue). The 6 data points are acquired from the same fully sampled *in vivo* spectrum of sample 1 with NSA = 8, 16, 32, 64 and 124, respectively.

> REPLACE THIS LINE WITH YOUR MANUSCRIPT ID NUMBER (DOUBLE-CLICK HERE TO EDIT) <

with the method from [18], QNet has MAPEs smaller for tCho, Glx, tCr and ml, but slightly larger for tNAA. The comparisons may indicate QNet outperforms the methods from [27] and [18].

E. Comparison with End-to-End QNet

The generalization ability of deep learning methods with LLS or the end-to-end manner is tested here. Only the range of NAA for the test data was changed to an abnormal range of 0.5-2.0 mM. An end-to-end QNet, which has another module of 6 SCBs with the same settings as the MM prediction module, was built to estimate metabolite concentrations directly from the network. Fig. 9 shows that when a metabolite concentration is not within the range set for trained data, the end-to-end manner cannot fit well and has quite a large fitting residual, while the QNet with LLS can still have an accurate fit with a small residual.

VI. LIMITATIONS OF THIS WORK

There are the challenging peaks difficult to quantify. It is still not very accurate to quantify some metabolites which are weak or overlapped with other strong resonance signals (e.g., Ala, Asp, Lac, GABA, etc.), and distinguish the metabolites with

similar structures (e.g., NAAG and NAA, Cr and PCr, etc.) with QNet. At a clinical magnetic field strength of 3.0 T, it is still difficult to distinguish them from each other by the spectrum

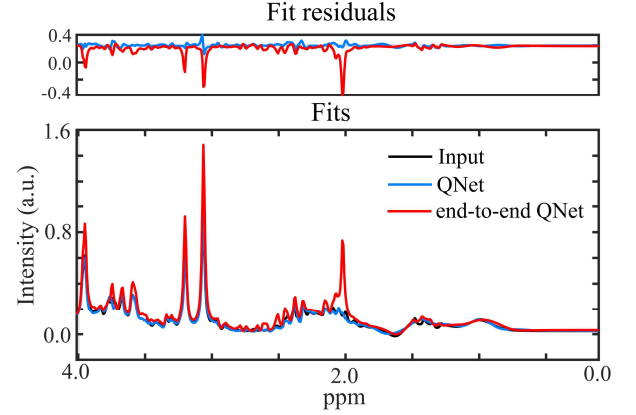


Fig. 9. Comparison between the two QNets with and without end-to-end manner. The range of NAA for the test data was changed from the normal 9.5-17 mM to abnormal 0.5-2.0 mM.

TABLE I 100 × SD of *In Vivo* Spectra with NSA = 8, 16, 32, 64, 96 AND 124

Sample No.	tNAA/tCr		ml/tCr		Glx/tCr		tCho/tCr		GSH/tCr	
	LCModel	QNet	LCModel	QNet	LCModel	QNet	LCModel	QNet	LCModel	QNet
1 (Fig. 8)	1.76	0.30	2.61	2.04	22.63	2.33	0.66	0.39	5.69	1.47
2	3.80	3.78	6.29	2.50	9.32	1.68	1.58	0.21	2.00	0.20
3	3.47	1.37	2.94	2.01	15.40	0.64	1.30	0.08	3.86	1.39
4	2.61	2.21	2.96	2.01	18.19	4.78	0.65	0.05	2.75	0.67
5	1.58	3.29	3.38	2.45	25.07	6.43	0.34	0.15	2.34	1.51
6	1.95	1.30	4.18	2.15	15.72	6.57	1.16	0.58	2.04	1.04
7	5.89	1.51	3.23	1.89	7.66	1.35	1.70	0.14	3.98	0.80
8	3.01	0.86	8.57	1.66	19.70	1.97	0.74	0.12	3.36	0.83
9	0.53	1.37	5.46	2.36	9.70	1.13	1.04	0.31	2.70	1.28
10	1.30	1.42	1.26	3.72	12.31	0.59	0.92	0.07	2.13	0.25
11	2.45	2.50	9.92	4.01	11.51	5.45	1.82	0.23	1.26	1.50
12	14.21	0.96	1.95	2.04	11.38	4.35	0.55	0.29	1.86	0.75
13	1.65	0.61	2.33	1.72	12.73	3.87	1.14	0.20	4.16	1.39
14	2.27	0.63	10.39	3.06	9.62	2.08	1.49	0.27	2.84	1.44
15	4.92	1.30	1.36	2.46	15.18	1.52	0.77	0.22	2.41	1.86
16	0.92	1.28	2.28	1.56	11.79	2.16	0.61	0.23	2.84	1.81
17	1.98	1.98	2.16	0.66	12.04	3.30	0.80	0.54	0.60	2.00
18	3.79	1.70	1.68	2.05	6.73	3.96	0.80	0.21	0.87	0.84
19	1.92	0.75	2.91	1.91	19.99	5.57	1.33	0.10	0.54	0.84
20	2.44	1.22	1.48	1.18	9.33	3.77	0.96	0.14	2.28	1.67
QNet score	16/20		17/20		20/20		19/20		17/20	

Note: Lower SD are highlighted in bold and we counted the scores (last row) of the SD of QNet is lower than that of LCModel in 20 *in vivo* spectra.

TABLE II COMPARISONS OF QNET WITH THE TWO DEEP LEARNING QUANTIFICATION METHODS.

Method	SNR definition	Metabolite	SNR range of simulated data	SMAPE or MAPE	
				The compared method	QNet
From [27] (10 ⁴ data)	$SNR_{FID} = \frac{[iff](y)_{first}}{\sigma'_{noise}}$	NAA	SNR _{FID} = 10	18.95	1.98
		NAAG		16.03	13.98
		Cr		19.64	2.98
		PCr		19.39	5.02
		GPC		13.67	11.86
		PCCh		14.27	12.05
		Glu		22.29	4.76
		Gln		22.98	6.87
		ml	20.20	2.84	
From [18] (5000 data)	$SNR_x = \frac{\max(y[x_k^1, x_k^2])}{\sigma_{noise}}$	tNAA	[6.90, 20.74]	4.00% ± 3.38%	4.35% ± 2.76%
		tCr	[6.84, 18.26]	3.66% ± 3.05%	2.41% ± 1.43%
		tCho	[7.05, 15.19]	7.87% ± 7.35%	2.59% ± 1.57%
		Glx	[5.28, 9.48]	5.36% ± 4.48%	4.56% ± 2.73%
		ml	[6.23, 13.32]	7.61% ± 6.77%	7.47% ± 4.81%

Note: SMAPE/MAPE is used for the comparison with the method in [27]/[18], respectively. Lower errors are highlighted in bold.

> REPLACE THIS LINE WITH YOUR MANUSCRIPT ID NUMBER (DOUBLE-CLICK HERE TO EDIT) <

obtained with the standard point resolved spectroscopy sequence excitation. Therefore, simulation of the MRS data acquired from specific sequences (e.g., MEGA- point-resolved spectroscopy sequence which is designed specifically to measure GABA) to train QNet is expected to address this difficulty.

Diversity of the training data is limited. Extension of the diversity of the simulated data is necessary. Since the simulated data used in this work are referenced from the literature all with healthy subjects, more data from unhealthy brains need to be collected, and the ranges of metabolite concentrations need to be updated. Or transfer learning can be applied to QNet to obtain a new quantification model suitable for both healthy and unhealthy brain MRS data to promote clinical applications.

Absolute concentration quantification is expected. Only relative concentrations of metabolites are presented. This approach may be limited by the stability of tCr level in subjects. Absolute quantification of metabolites is more challenging but may provide quantitative diagnosis report for patients.

VII. CONCLUSION

In this work, we proposed the MRS Quantification deep learning Network (QNet). It combines the superior nonlinear learning capability of neural networks and the effectiveness of Linear Least Squares (LLS). The training data is generated as practically as possible through simulating the metabolite basis-set with the physics-informed quantum mechanical and exponential model, and incorporating practical metabolite concentration ranges, imperfection factors, macromolecular background signal and noise. QNet first applied multi-layer convolutions to predict the imperfection factors and the macromolecular background signal separately to simplify the problem of least squares from complicated nonlinearity to simple linearity, and then LLS is applied to linearly estimate individual metabolite concentrations. This special strategy improves the generalization of the common end-to-end deep learning method. Results show that QNet can achieve lower quantification errors than LCMoel for most (80%) metabolites on the simulated data, especially in the low signal-to-noise levels. For the healthy *in vivo* data, QNet gets the quantification results that are highly consistent with those of LCMoel in the case of high signal-to-noise level, and achieves more stable quantification at low signal-to-noise level. In summary, this study provides an intelligent, reliable and robust MRS quantification method. QNet has been deployed on a cloud computing platform, CloudBrain-MRS, which is open accessed at <https://csrc.xmu.edu.cn/CloudBrain.html>.

REFERENCES

- [1] R. A. De Graaf, *In Vivo NMR Spectroscopy: Principles and Techniques*: John Wiley & Sons, 2019.
- [2] D. Bertholdo, A. Watcharakorn, and M. Castillo, "Brain proton magnetic resonance spectroscopy: introduction and overview," *Neuroimag. Clin. N. Am.*, vol. 23, no. 3, pp. 359-380, 2013.
- [3] F. Cooke, A. Blamire, D. Manners, P. Styles, and B. Rajagopalan, "Quantitative proton magnetic resonance spectroscopy of the cervical spinal cord," *Magn. Reson. Med.*, vol. 51, no. 6, pp. 1122-1128, 2004.
- [4] F. Fischbach, T. Schirmer, M. Thormann, T. Freund, J. Ricke, and H. Bruhn, "Quantitative proton magnetic resonance spectroscopy of the normal liver and malignant hepatic lesions at 3.0 Tesla," *Eur. Radio.*, vol. 18, no. 11, pp. 2549-2558, 2008.
- [5] L. Kwock, J. K. Smith, M. Castillo, M. G. Ewend, F. Collichio, D. E. Morris, T. W. Bouldin, and S. Cush, "Clinical role of proton magnetic resonance spectroscopy in oncology: brain, breast, and prostate cancer," *Lancet Oncol.*, vol. 7, no. 10, pp. 859-868, 2006.
- [6] S. W. Provencher, "Estimation of metabolite concentrations from localized *in vivo* proton NMR spectra," *Magn. Reson. Med.*, vol. 30, no. 6, pp. 672-679, 1993.
- [7] G. Helms, "Analysis of 1.5 Tesla proton MR spectra of human brain using LCMoel and an imported basis set," *Magn. Reson. Imaging*, vol. 17, no. 8, pp. 1211-1218, 1999.
- [8] Q. Yang, Z. Wang, K. Guo, C. Cai, and X. Qu, "Physics-driven synthetic data learning for biomedical magnetic resonance: the imaging physics-based data synthesis paradigm for artificial intelligence," *IEEE Signal Process Mag.*, vol. 40, no. 2, pp. 129-140, 2023.
- [9] F. Lam, X. Peng, and Z. P. Liang, "High-dimensional MR spatio-spectral imaging by integrating physics-based modeling and data-driven machine learning: current progress and future directions," *IEEE Signal Process Mag.*, vol. 40, no. 2, pp. 101-115, 2023.
- [10] S. Smith, T. Levante, B. H. Meier, and R. R. Ernst, "Computer simulations in magnetic resonance. An object-oriented programming approach," *J. Magn. Reson., Ser. A*, vol. 106, no. 1, pp. 75-105, 1994.
- [11] R. Simpson, G. A. Devenyi, P. Jezzard, T. J. Hennessy, and J. Near, "Advanced processing and simulation of MRS data using the FID appliance (FID-A) -an open source, MATLAB-based toolkit," *Magn. Reson. Med.*, vol. 77, no. 1, pp. 23-33, 2017.
- [12] D. Graverondemilly, A. Diop, A. Briguet, and B. Fenet, "Product-operator algebra for strongly coupled spin systems," *J. Magn. Reson., Ser. A*, vol. 101, no. 3, pp. 233-239, 1993.
- [13] F. Lam, Y. Li, and X. Peng, "Constrained magnetic resonance spectroscopic imaging by learning nonlinear low-dimensional models," *IEEE Trans. Med. Imaging*, vol. 39, no. 3, pp. 545-555, 2019.
- [14] E. C. Craig, and A. G. Marshall, "Automated phase correction of FT NMR spectra by means of phase measurement based on dispersion versus absorption relation (DISPA)," *J. Magn. Reson.*, vol. 76, no. 3, pp. 458-475, 1988.
- [15] J. Near, A. D. Harris, C. Juchem, R. Kreis, M. Marjańska, G. Öz, J. Slotboom, M. Wilson, and C. Gasparovic, "Preprocessing, analysis and quantification in single-voxel magnetic resonance

> REPLACE THIS LINE WITH YOUR MANUSCRIPT ID NUMBER (DOUBLE-CLICK HERE TO EDIT) <

- spectroscopy: experts' consensus recommendations," *NMR Biomed.*, vol. 34, no. 5, pp. e4257, 2021.
- [16] M. I. Osorio Garcia, D. Sima, F. Nielsen, U. Himmelreich, and S. Van Huffel, "Quantification of magnetic resonance spectroscopy signals with lineshape estimation," *J. Chemom.*, vol. 25, no. 4, pp. 183-192, 2011.
- [17] H. J. Zöllner, M. Považan, S. C. Hui, S. Tapper, R. A. Edden, and G. Oeltzschner, "Comparison of different linear-combination modeling algorithms for short-TE proton spectra," *NMR Biomed.*, vol. 34, no. 4, pp. e4482, 2021.
- [18] H. H. Lee, and H. Kim, "Intact metabolite spectrum mining by deep learning in proton magnetic resonance spectroscopy of the brain," *Magn. Reson. Med.*, vol. 82, no. 1, pp. 33-48, 2019.
- [19] H. Ratiney, M. Sdika, Y. Coenradie, S. Cavassila, D. v. Ormond, and D. Graveron Demilly, "Time-domain semi-parametric estimation based on a metabolite basis set," *NMR Biomed.*, vol. 18, no. 1, pp. 1-13, 2005.
- [20] J. B. Pouillet, D. M. Sima, A. W. Simonetti, B. De Neuter, L. Vanhamme, P. Lemmerling, and S. Van Huffel, "An automated quantitation of short echo time MRS spectra in an open source software environment: AQSES," *NMR Biomed.*, vol. 20, no. 5, pp. 493-504, 2007.
- [21] G. Reynolds, M. Wilson, A. Peet, and T. N. Arvanitis, "An algorithm for the automated quantitation of metabolites in in vitro NMR signals," *Magn. Reson. Med.*, vol. 56, no. 6, pp. 1211-1219, 2006.
- [22] M. Marjańska *et al.*, "Results and interpretation of a fitting challenge for MR spectroscopy set up by the MRS study group of ISMRM," *Magn. Reson. Med.*, vol. 87, no. 1, pp. 11-32, 2022.
- [23] D. Chen *et al.*, "Magnetic resonance spectroscopy deep learning denoising using few in vivo data," *IEEE Trans. Comput. Imaging*, vol. 9, pp. 448-458, 2023.
- [24] D. Chen, Z. Wang, D. Guo, V. Orekhov, and X. Qu, "Review and prospect: deep learning in nuclear magnetic resonance spectroscopy," *Chem. Eur. J.*, vol. 26, no. 46, pp. 10391-10401, 2020.
- [25] Y. Li, Z. Wang, R. Sun, and F. Lam, "Separation of metabolites and macromolecules for short-TE ¹H-MRSI using learned component-specific representations," *IEEE Trans. Med. Imaging*, vol. 40, no. 4, pp. 1157-1167, 2021.
- [26] Y. Huang, J. Zhao, Z. Wang, V. Orekhov, D. Guo, and X. Qu, "Exponential signal reconstruction with deep hankel matrix factorization," *IEEE Trans. Neural Networks Learn. Syst.*, DOI: 10.1109/TNNLS.2021.3134717, 2021.
- [27] N. Hatami, M. Sdika, and H. Ratiney, "Magnetic resonance spectroscopy quantification using deep learning," in *International Conference on Medical Image Computing and Computer-Assisted Intervention*, pp. 467-475, 2018.
- [28] Z. Wang *et al.*, "A sparse model-inspired deep thresholding network for exponential signal reconstruction-application in fast biological spectroscopy," *IEEE Trans. Neural Networks Learn. Syst.*, DOI: 10.1109/TNNLS.2022.3144580, 2022.
- [29] J. Songeon, S. Courvoisier, L. Xin, T. Agius, O. Dabrowski, A. Longchamp, F. Lazeyras, and A. Klauser, "In vivo magnetic resonance ³¹P-spectral analysis with neural networks: ³¹P-SPAWN," *Magn. Reson. Med.*, vol. 89, no. 1, pp. 40-53, 2022.
- [30] X. Qu, Y. Huang, H. Lu, T. Qiu, D. Guo, T. Agback, V. Orekhov, and Z. Chen, "Accelerated nuclear magnetic resonance spectroscopy with deep learning," *Angew. Chem. Int. Ed.*, vol. 59, no. 26, pp. 10297-10300, 2019.
- [31] Z. Iqbal, D. Nguyen, M. A. Thomas, and S. Jiang, "Deep learning can accelerate and quantify simulated localized correlated spectroscopy," *Sci. Rep.*, vol. 11, no. 1, pp. 8727, 2021.
- [32] A. Cárdenas Blanco, C. Tejos, P. Irrarazaval, and I. Cameron, "Noise in magnitude magnetic resonance images," *Concepts Magn. Reson. Part A*, vol. 32, no. 6, pp. 409-416, 2008.
- [33] V. Govindaraju, K. Young, and A. A. Maudsley, "Proton NMR chemical shifts and coupling constants for brain metabolites," *NMR Biomed.*, vol. 13, no. 3, pp. 129-153, 2000.
- [34] I. Tkáč, G. Öz, G. Adriany, K. Uğurbil, and R. Gruetter, "In vivo ¹H NMR spectroscopy of the human brain at high magnetic fields: metabolite quantification at 4T vs. 7T," *Magn. Reson. Med.*, vol. 62, no. 4, pp. 868-879, 2009.
- [35] R. Birch, A. C. Peet, H. Dehghani, and M. Wilson, "Influence of macromolecule baseline on ¹H MR spectroscopic imaging reproducibility," *Magn. Reson. Med.*, vol. 77, no. 1, pp. 34-43, 2017.
- [36] K. L. Behar, D. L. Rothman, D. D. Spencer, and O. A. Petroff, "Analysis of macromolecule resonances in ¹H NMR spectra of human brain," *Magn. Reson. Med.*, vol. 32, no. 3, pp. 294-302, 1994.
- [37] K. S. Opstad, B. A. Bell, J. R. Griffiths, and F. A. Howe, "Toward accurate quantification of metabolites, lipids, and macromolecules in HRMAS spectra of human brain tumor biopsies using LCMoel," *Magn. Reson. Med.*, vol. 60, no. 5, pp. 1237-1242, 2008.
- [38] P. A. Bottomley, "Spatial localization in NMR spectroscopy in vivo," *Ann. N. Y. Acad. Sci.*, vol. 508, no. 1, pp. 333-348, 1987.
- [39] T. L. Hwang, and A. J. Shaka, "Water suppression that works. excitation sculpting using arbitrary waveforms and pulsed-field gradients," *J. Magn. Reson., Ser. A*, vol. 112, no. 2, pp. 275-279, 1995.